

Received: 2016.05.20  
Accepted: 2016.07.18  
Published: 2017.03.31

# Vascularization Potential of Electrospun Poly(L-Lactide-co-Caprolactone) Scaffold: The Impact for Tissue Engineering

Authors' Contribution:  
Study Design A  
Data Collection B  
Statistical Analysis C  
Data Interpretation D  
Manuscript Preparation E  
Literature Search F  
Funds Collection G

ABDEF 1,2 **Arkadiusz Jundziłł\***  
CDE 1 **Marta Pokrywczyńska\***  
BD 1 **Jan Adamowicz**  
BCDE 3 **Tomasz Kowalczyk**  
BD 4 **Maciej Nowacki**  
BD 5 **Magdalena Bodnar**  
BD 5,6 **Andrzej Marszałek**  
BD 7 **Małgorzata Frontczak-Baniewicz**  
BCD 3 **Grzegorz Mikułowski**  
BEF 1 **Tomasz Kloskowski**  
DEF 8 **James Gatherwright**  
CDEF 1,9 **Tomasz Drewa**

1 Chair of Urology, Department of Regenerative Medicine, Collegium Medicum, Nicolaus Copernicus University, Bydgoszcz, Poland  
2 Department of Plastic, Reconstructive and Aesthetic Surgery, Collegium Medicum, Nicolaus Copernicus University, Bydgoszcz, Poland  
3 Institute of Fundamental Technological Research, Polish Academy of Science, Warsaw, Poland  
4 Chair and Department of Surgical Oncology, Collegium Medicum, Nicolaus Copernicus University, Bydgoszcz, Poland  
5 Department of Clinical Pathomorphology, Collegium Medicum, Nicolaus Copernicus University, Bydgoszcz, Poland  
6 Department of Oncologic Pathology, Poznań University of Medical Sciences and Greater Poland Oncology Center, Poznań, Poland  
7 Electron Microscopy Platform, Mossakowski Medical Research Centre, Polish Academy of Sciences, Warsaw, Poland  
8 Department of Plastic Surgery, University Hospitals – Case Medical Center, Cleveland, OH, U.S.A.  
9 Department of Urology and Oncological Urology, Nicolaus Copernicus Hospital, Toruń, Poland

\* These two authors contributed equally during the preparation of the manuscript

**Corresponding Author:** Tomasz Kloskowski, e-mail: [tomaszkloskowski@op.pl](mailto:tomaszkloskowski@op.pl)  
**Source of support:** Departmental sources

**Background:** Electrospun nanofibers have widespread putative applications in the field of regenerative medicine and tissue engineering. When compared to naturally occurring collagen matrices, electrospun nanofiber scaffolds have two distinct advantages: they do not induce a foreign body reaction and they are not at risk for biological contamination. However, the exact substrate, structure, and production methods have yet to be defined.

**Material/Methods:** In the current study, tubular-shaped poly(L-lactide-co-caprolactone) (PLCL) constructs produced using electrospinning technology were evaluated for their potential application in the field of tissue regeneration in two separate anatomic locations: the skin and the abdomen. The constructs were designed to have an internal diameter of 3 mm and thickness of 200 μm. Using a rodent model, 20 PLCL tubular constructs were surgically implanted in the abdominal cavity and subcutaneously. The constructs were then evaluated histologically using electron microscopy at 6 weeks post-implantation.

**Results:** Histological evaluation and analysis using scanning electron microscopy showed that pure scaffolds by themselves were able to induce angiogenesis after implantation in the rat model. Vascularization was observed in both tested groups; however, better results were obtained after intraperitoneal implantation. Formation of more and larger vessels that migrated inside the scaffold was observed after implantation into the peritoneum. In this group no evidence of inflammation and better integration of scaffold with host tissue were noticed. Subcutaneous implantation resulted in more fibrotic reaction, and differences in cell morphology were also observed between the two tested groups.

**Conclusions:** This study provides a standardized evaluation of a PLCL conduit structure in two different anatomic locations, demonstrating the excellent ability of the structure to achieve vascularization. Functional, histological, and mechanical data clearly indicate prospective clinical utilization of PLCL in critical size defect regeneration.

**MeSH Keywords:** **Polymers • Regenerative Medicine • Tissue Engineering • Tissue Scaffolds • Urinary Diversion**

**Full-text PDF:** <http://www.medscimonit.com/abstract/index/idArt/899659>

 4368  1  6  40



## Background

The “holy grail” of tissue engineering is the ability to artificially create biologically solvent constructs that can permanently replace deficient or lost biologic structures. One of the rate-limiting factors in making the translational step from the laboratory to clinical application is the relatively deficient blood supply of implanted materials [1]. Insufficient vascularity can either lead to inadequate integration or even construct destruction due to a lack of infiltration by host cells. Therefore, biologic constructs should be able to induce a rapid but organized invasion of host cells and tissues in order to create the metabolic milieu necessary for successful incorporation [2]. Electrospun nanofibers have been extensively studied for their potential applications in regenerative medicine, tissue engineering, and drug delivery systems. The most significant factors in scaffold design determining its vascularization after implantation are the use of the proper material and the fabrication technique. The extracellular matrix (ECM, fiber thickness 50–500 nm) structure can be successfully reproduced using electrospinning nanofiber technology [3]. Artificially created scaffolds provide distinct advantages compared to natural collagen matrices: they are significantly less likely to produce a foreign body or immunologic reaction, there is near zero risk of biologic contamination by transmitting infectious materials, and there is no limitation in donor availability, theoretically providing an endless supply of materials. In addition, the electrospun constructs are nearly identical between products, as opposed to biologics, which can have highly variable compositions based on a multitude of factors that are difficult to account for and control. Properties and dimensions of electrospun materials such as thickness, diameter, porosity, degradation rate, and so forth can be more readily controlled and tailored according to different applications. Electrospun nanofiber constructs also do not obstruct the flow of nutrients and oxygen to the cells, nor the removal of potentially noxious metabolites. The three-dimensional interaction of biologic materials is also often overlooked, and electrospun nanofibers can be tailored to any structural defect including biologic membranes, conduits, branching scaffolds, and so forth. The 3D structure of these implants can be critical for inducing appropriate cell integration, ingrowth, and construct function. Aliphatic polyesters including poly( $\epsilon$ -caprolactone) (PCL) and its copolymers have been widely used in tissue engineering, with both *in vitro* and *in vivo* studies demonstrating their potential as biologic scaffolds [4–6].

While their theoretical advantage is huge, more study is required to understand the best materials, production, structure, and application of different electrospun materials. To that end, the current study aims to characterize the successful vascular integration of a uniquely constructed tubular-shaped poly(L-lactide-co-caprolactone) (PLCL) implant produced using

electrospinning technology in two separate anatomic locations: the subcutaneous soft tissue and the abdomen using a rodent model.

## Material and Methods

### Material design

Poly(L-lactide-co-caprolactone) (PLCL) (Purac, Gorinchem, Netherlands), chloroform (CHCl<sub>3</sub>) (POCH, Poland), and N,N-dimethylformamide (DMF) (POCH, Poland) were used [7]. Tubular nanofibrous conduits were produced using electrospinning technology [8]. Conduits were designed to have an internal diameter of 3 mm and a thickness of 200  $\mu$ m. The detailed electrospinning process has been previously described [9]. Briefly, PLCL was dissolved in a mixture of CHCl<sub>3</sub> and DMF (mass proportion 16: 1) to form a 9% solution that was left overnight. Electrospinning was conducted in a custom-made polycarbonate chamber of approximate 1 cubic meter in volume. The electrospinning setup consisted of a custom-made voltage power supply with an adjustable voltage output. The electrospun solution was left overnight to ensure polymer chain disentanglement. The solution was transferred from a metering syringe pump (New Era Pumping Systems, GB) through a hydraulic system to a nozzle consisting of a blunt needle (outer volume 0.4 mm) connected to a high voltage supply. Grounded aluminum foil attached to a rotating brass shaft served as a target. Tubes of electrospun nanofibers were left overnight for material relaxation, immersed in water for several minutes, and carefully stripped from the shaft [10].

In the current study a spinning distance of 20 cm, an electric potential of 15 kV, and a solution throughput of 0.500  $\mu$ L/h was used. A rotating brass rod (1000 rpm, diameter of 4 mm) served as a nanofibrous mat collector. The polymer used for electrospinning was PLCL, which was composed of 70% L-lactide and 30% caprolactone units and is known commercially as Purasorb 7015 (Purac Biochem BV, Gorinchem, Netherlands). The electrospinning solution was made of 9% polymer dissolved in a mixture of solvents (chloroform + dimethylformamide; mass proportions 16: 1). A scanning electron microscopy (SEM) analysis was performed to visualize the biomaterial structure (Figure 1A, 1B) [10].

### Experimental groups

Twenty male Wistar rats weighing 270–320 g were used. Animals were divided into two equal groups. In group 1 the scaffolds were implanted in the abdominal cavity. In group 2 the biomaterials were implanted in the subcutaneous dorsal skin.

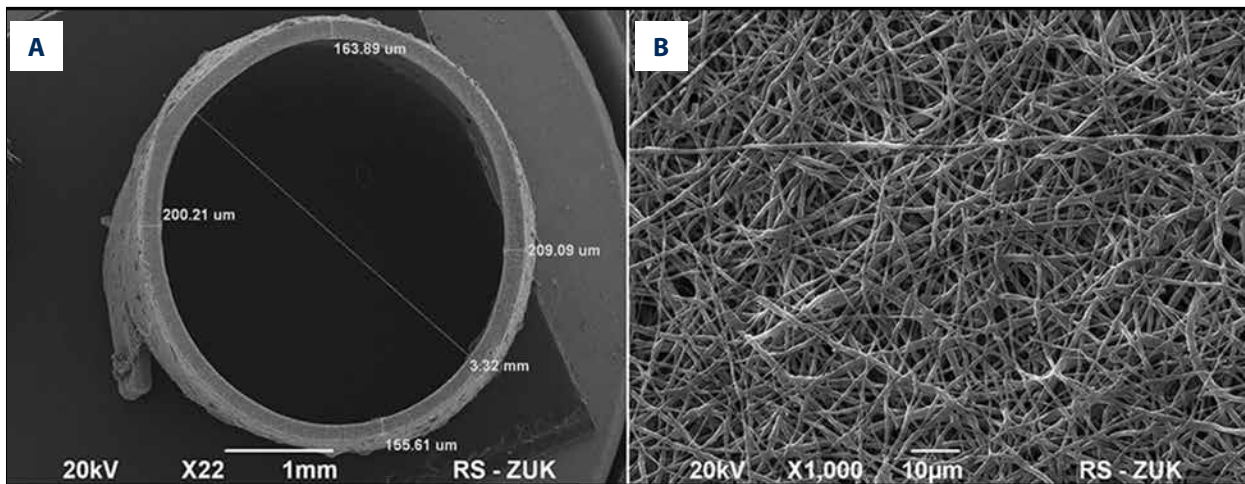


**Figure 1.** Scanning electron microscopy image of PLCL tubular scaffold. (A) Front view. The scaffold has a lumen of ca. 3.3 mm and a thickness of 0.155–0.209 mm. (B) Surface view. Structure rich in pores formed of fibers ranging in diameter from a fraction of a micrometer to ca. 2  $\mu$ m is shown.

### Surgical procedure of PLCL scaffold implantation

After induction of anesthesia, group 1 animals were placed in the supine position. Then the abdomen was shaved and prepped with povidone-iodine solution. A median skin incision was made above and under the umbilicus. The abdominal muscular structure was separated, the peritoneum was incised, and the abdominal cavity was entered. Employing two saline-wetted, cotton-tipped applicators, the rat was gently eviscerated. After moving the rat into a supine position, the contralateral side (with both sides chosen randomly) was operated on. The PLCL conduits were surgically affixed to the internal part of the abdominal wall by single nonabsorbable interrupted sutures 5-0. The muscle, peritoneum, and skin were repaired in two layers with a running 4-0 absorbable suture. In group 2, after induction of anesthesia, rats were placed in the prone position and a midline skin incision was performed approximately 2–3 cm above and under vertebrae L1–L2. The PLCL scaffolds were fastened to the subcutaneous tissue using a single nonabsorbable 5-0 suture. The skin was then closed with a single, continuous 4-0 absorbable suture.

Six weeks after PLCL scaffold implantation, both rat groups were euthanized. Implanted biomaterials were removed and fixed in 10% buffered Formalin solution for histological evaluation.

### Animal care

Animals used in this study received humane care in accordance with the guidelines set forth by the National Institutes of Health regarding the Care and Use of Laboratory Animals. The protocol was approved by the Committee on the Ethics of Animal Experiments of the University of Technology and Life Science in Bydgoszcz, Poland (26/2013). Animals were caged at room

temperature with a 12-hour light/dark cycle. Standard laboratory food and water were available ad libitum. Operations were performed using a standard anesthesia cocktail of ketamine (30 mg/kg), xylazine (6 mg/kg), and acepromazine (1 mg/kg). Post-operative analgesia was maintained with non-steroidal anti-inflammatory drugs and paracetamol-based pain killers. Euthanasia was induced using an accepted, standardized protocol by injecting an intraperitoneal barbiturate overdose (100 mg/kg). No eating, sleeping, or behavioral abnormalities were observed in either experimental group. All animals survived the operation protocol, and in all cases the implantation sites and surgical wounds healed without incident.

### Method of transmission electron microscopy (TEM) analysis of electrospun nanofibers

Samples were prepared with a “regular” ice-cold fixative with 2% paraformaldehyde and 2.5% glutaraldehyde in 0.1 M cacodylate buffer at a pH of 7.4. The specimens were handled with the typical ice-cold fixative post-fixed in 1% (w/v) OsO<sub>4</sub> solution in deionized water, dehydrated in an ethanol gradient, and encased in an epoxy resin (Epon 812). Ultrathin (60 nm) sections were prepared as previously described [11]. Specimens were examined using a transmission electron microscope (JEM-1200EX, Jeol, Japan).

### Histological analysis

Specimens were fixed in 10% neutral buffered Formalin and embedded in paraffin. Cross-sections of the tubular scaffold with adjacent tissues in their entirety were prepared. Histological analysis with hematoxylin and eosin (HE) staining was performed.

## Immunohistochemical analysis

Immunohistochemical staining was performed on 3 µm paraffin tissue sections according to a previously standardized protocol [12]. Epitopes were unmasked using Epitope Retrieval Solution (high pH) with PT-Link (Dako, Denmark) and incubated with primary antibody for 20 minutes at room temperature. The primary mouse monoclonal antibody against CD31, Clone JC70A (dilution: RTU, Dako, Denmark) was used. For identification of the specific antigen-antibody complex, EnVision FLEX Anti-Mouse HRP System (Dako, Denmark) and 3-3'-diaminobenzidine (DAB) as a substrate for horseradish peroxidase were used. Finally, the sections were counterstained with hematoxylin, dehydrated in increasing grades of ethyl alcohol (80%, 90%, 96%, 99.8%), and mounted with Shandon Consul Mount (Thermo Fisher Scientific, Waltham, Massachusetts, USA). The expression of analyzed antigens was indicated by the presence of a brown reaction product.

## The evaluation of vessel density

The level of CD31 protein expression was used to measure vessel density via an automated morphometric tool in the Image J program (USA). Analysis of average vessel density was performed in three randomly selected areas at 20× the original magnification using a light microscope ECLIPSE E800 (Nikon Instruments Europe, Germany). The microphotographs were taken using a Nikon Digital Sight DS-5Mc camera (Nikon Instruments Europe, Germany) driven by 4NIS Elements F 3.0 software (Nikon Instruments Europe, Germany). The analyzed images included the area of positively stained endothelial cells and level of CD31 expression (0–3). The analysis of the average vessel density was performed in each case in 3 hot spots. The morphometrical analysis of CD31 expression was calculated as the ratio of the area of positively stained endothelial cells (scale: 0–100) and the level of CD31 expression (scale: 0–255).

## Mechanical properties of the PLCL biomaterial

The geometry and structure of the fibers of the examined specimen were measured by SEM and its dimensions were as follows: diameter: 4 mm, thickness: 0.200 mm, and length: 25 mm. A tensile strength test was also conducted on a load frame of a servohydraulic material testing machine (MTS 242.01 actuator, Eden Prairie, Minnesota, USA). The specimen was mounted into flat grips with a gauge base of 12.5 mm. During the test, the specimen was longitudinally extracted at a rate of 0.3 mm/s to failure. The grip travel and specimen load were continuously measured throughout the duration of the procedure with a precision force transducer (Interface, model 1500, measuring range 125 N, resolution 0.0625 N) and an MTS system linear variable differential transformer (measuring range 100 mm, resolution 0.01 mm).

Stress/strain curves for the specimens were generated, and the ultimate tensile strength, maximum strain, and elastic modulus were determined. The strength (MPa) was calculated by dividing the value of the failure load by the initial cross-sectional area of the specimen. The maximum strain (the strain value corresponding to the ultimate stress) was calculated as the elongation of the specimen divided by the initial gauge length (mm/mm). The elastic modulus (MPa) was defined as the slope of the linear regions of the stress/strain curve.

## Statistical analysis

Parametric and nonparametric applied significance tests were used to verify hypotheses. A non-parametric Shapiro-Wilk test was used to verify the hypothesis of normal distribution of the studied traits. A Snedecor F test was used to verify the hypothesis of homogeneity of variance in the two treatment groups. A parametric Cochran-Cox test was used to compare mean values in the two groups having different variances.

## Results

### Macroscopic evaluation of PLCL conduit neo-angiogenesis by anatomic location

There was a clear difference in the amount of host angiogenic invasion into the PLCL conduits based on anatomic placement. In the current model, there was significantly more vascularization when the PLCL scaffold was implanted intraperitoneally compared to subcutaneous placement. The intraperitoneal cavity guarantees free access to a considerably developed omentum vascular network. Moreover, after PLCL scaffold transplantation, interstitial fluid diffusion can alert immune response signals. The combination of intraperitoneal fluids and the omentum network can be an irreplaceable bioreactor for biomaterial vascularization. Clinical evaluation at 6 weeks demonstrated gross evidence of PLCL conduit vascularization. The long omentum vascular pedicle incorporated with PLCL offers an easy transposition of biomaterials to cover the defect without the hazard of loss of blood supply. Moreover, cells that spontaneously penetrate between fibers during the procedure and exist in omentum fluid secrete cytokines under the influence of hypoxia, which accelerates the neovascularization.

After implantation of tissue-engineered constructs under the skin, we observed spontaneous vascularization in relation to the intensified inflammatory wound healing response induced by the surgical procedure. The subcutis environment is less advantageous for spontaneous vessel formation, which was clearly observed in our study (Figures 2, 3).

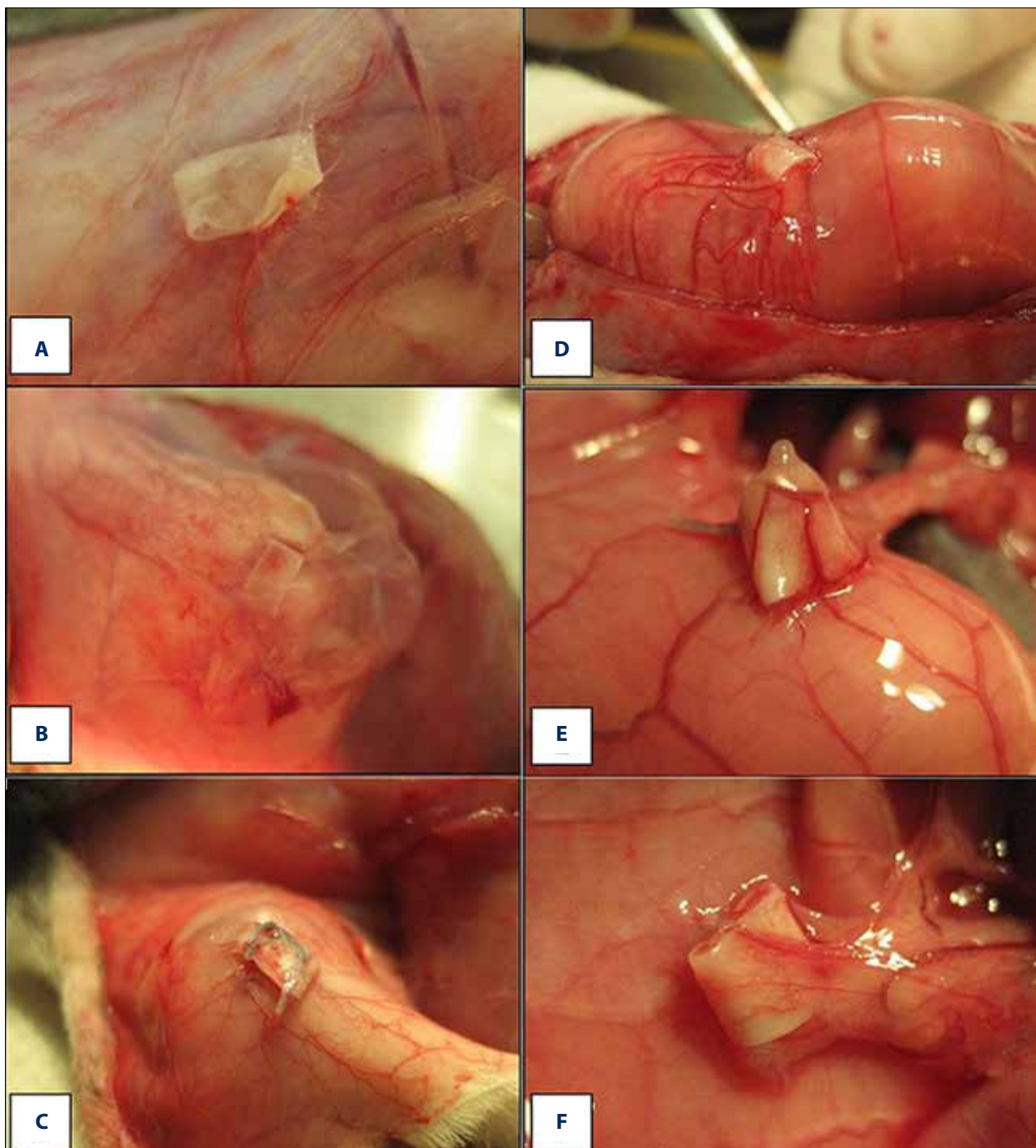


**Figure 2.** Clinical biomaterial evaluation. Results from groups 1 and 2 six weeks following surgical implantation of PLCL conduits. Macroscopic assessments of group 1 (subcutaneous placement) samples can be seen on slides (A–C); while slides (D–F) represent group 2 samples (intraperitoneal placement). Group 1 demonstrated less vascular density and smaller vessel diameter when compared to group 2. Group 1 also demonstrated more evidence of inflammation.

The subcuticular group (group 1) was associated with less vascular incorporation when compared to the intraperitoneal group. This was histologically demonstrated in group 1, which had significantly less vascular density and a smaller diameter of vessels.

#### **Histological analysis of implanted PLCL**

Conduit host angiogenesis varied between the two transplanted groups, as did microcapillary formation.

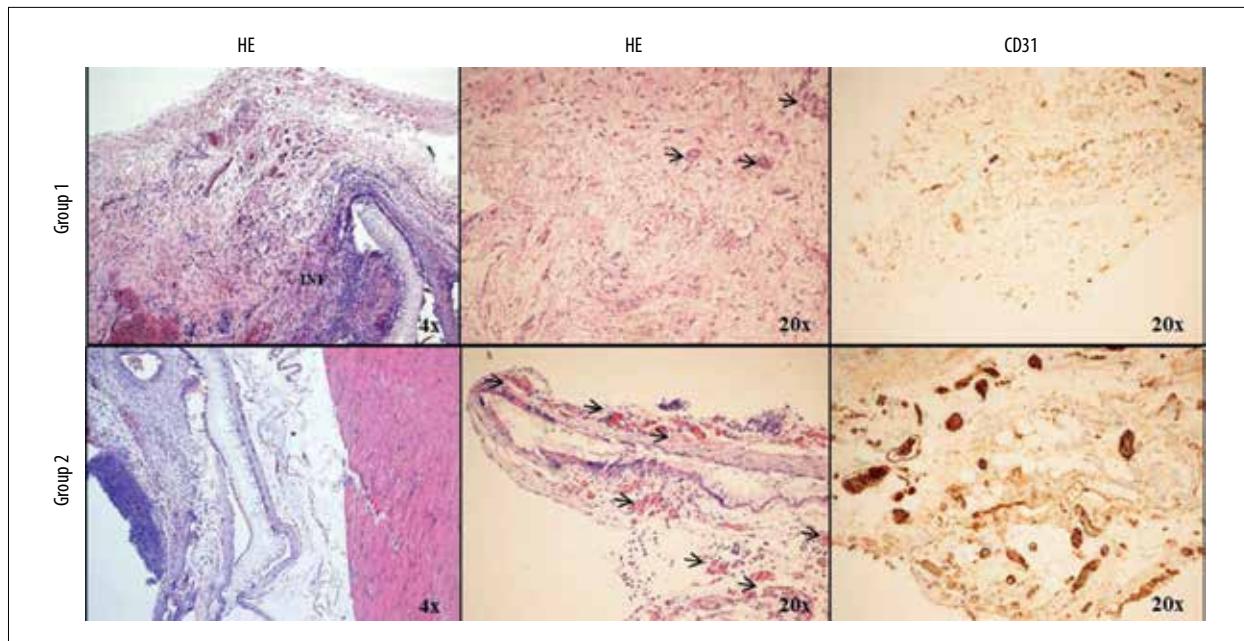


**Figure 3.** Histological comparison of blood vessel density. Six weeks following PLCL implantation, tissue samples were processed and subjected to histological staining (hematoxylin and eosin staining as well as CD31 staining). INF indicates an intensified inflammation process in the direct vicinity of the PLCL biomaterial. The arrows indicate localization of vessel groups near the scaffold. Magnification is shown in the right corner of the images.

In all groups, the PLCL biomaterial appeared to stimulate capillaries' growth and neo-vascularization. Microcapillary-like structures of endothelial cells were observed covering the scaffold lumen. Vasculature migration was also seen intertwined between PLCL scaffold fibers.

In contrast, when conduits were placed in the subcutaneous tissue, vessels were found mostly on the exterior scaffold surface. Moreover, vessels grew and spread only on the fibers and did not propagate into the surrounding tissues or into the space between fibers. There was also histological evidence of a low-grade inflammatory response. The inflammatory response was mainly responsible for low-grade vascularization in subcutis PLCL implantation. In contrast, scaffolds that were placed intraperitoneally demonstrated better integration and a higher density of vascularized connective tissue without evidence of inflammation. Microcapillary structures were observed on the surface of silk fibroin as well as inside the scaffold. Besides vascular structures, PLCL exhibited a unobstructed and perfused lumen, confirmed by presence of erythrocytes within it. PLCL seemed to have a beneficial effect on the vascular structure formation in the adjacent implant tissue.

Microscopic evaluation of intraperitoneal samples demonstrated fully developed arterial walls and a homogenous vascularization consisting partially of prominent vessels. Microcapillary-like structures and even 3 vessel layers intertwined throughout the biomaterials were also present. The average vessel size was

statistically larger in the intraperitoneal group compared to the group with subcutaneously placed conduits, with diameters measuring  $54 \pm 9.6$  versus  $38 \pm 15.2$   $\mu\text{m}$ , respectively ( $p < 0.0001$ ).

CD31 expression confirmed the presence of neovascular endothelium in both sample groups.

At 6 weeks post-transplantation, the PLCL conduit revealed a similar integration pattern into host tissues surrounded with a loose connective tissue. In both groups histological evaluation of the PLCL scaffold showed that fibers were well integrated into the surrounding peripheral tissues. However, the subcutaneous group demonstrated a significantly more fibrotic reaction when compared to the intraperitoneal group. There was also a discernible difference the cellular morphology when assessing the two groups. In the intraperitoneal group, cells displayed a higher degree of fibroblastic morphology with typical projections. In contrast, cells in the subcutaneous group exhibited a smaller, narrower, and more spherical morphology. Both conduits demonstrated a closely associated vascular network, as demonstrated by erythrocytes within luminal vascular structures. However, the degree/extent of the vascular networks was significantly more in the intraperitoneal group.

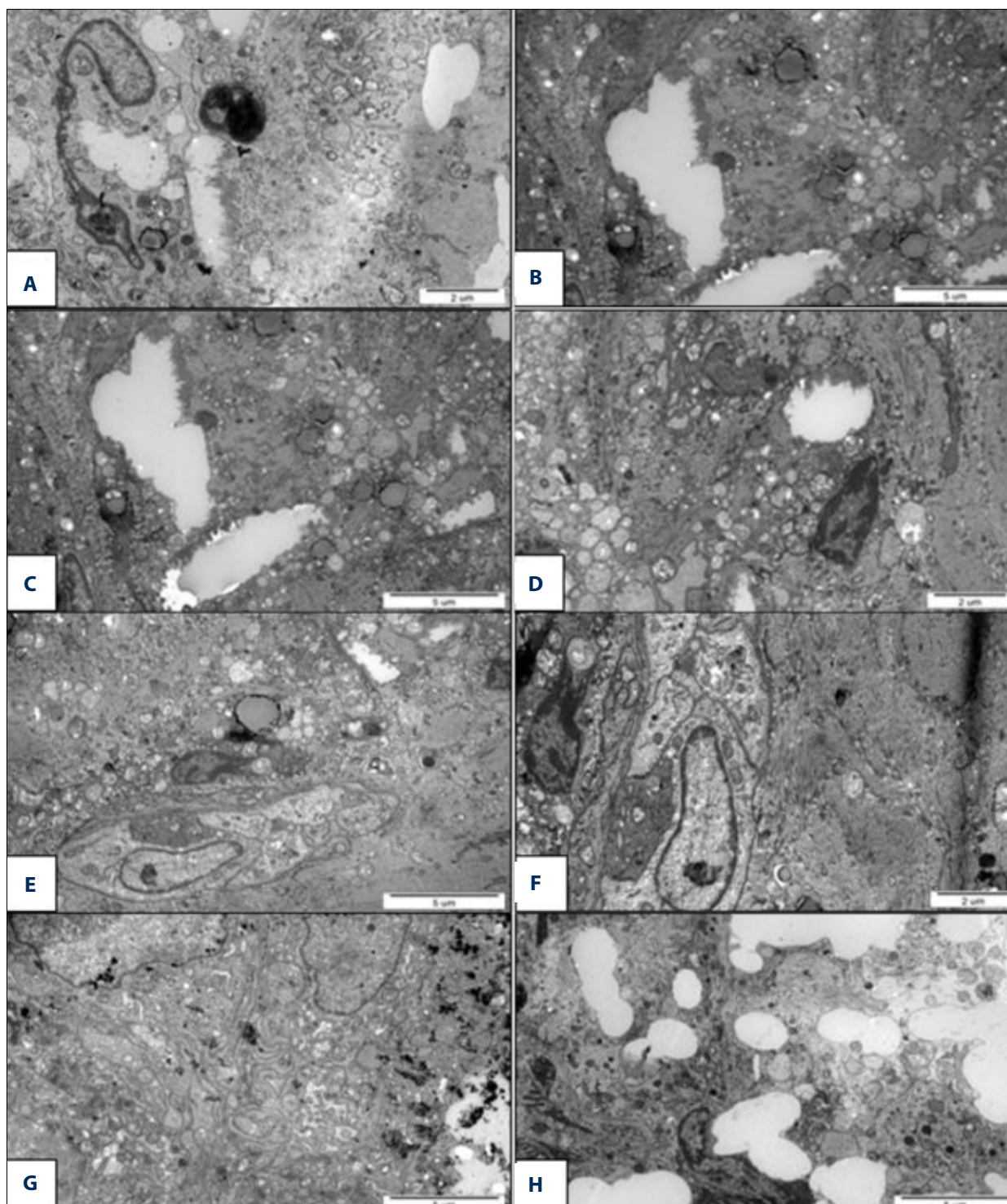


**Figure 4. (A–H)** Ultrastructural micrographs of a PLCL conduit following subcutaneous implantation. The presented images show results obtained 6 weeks after implantation.

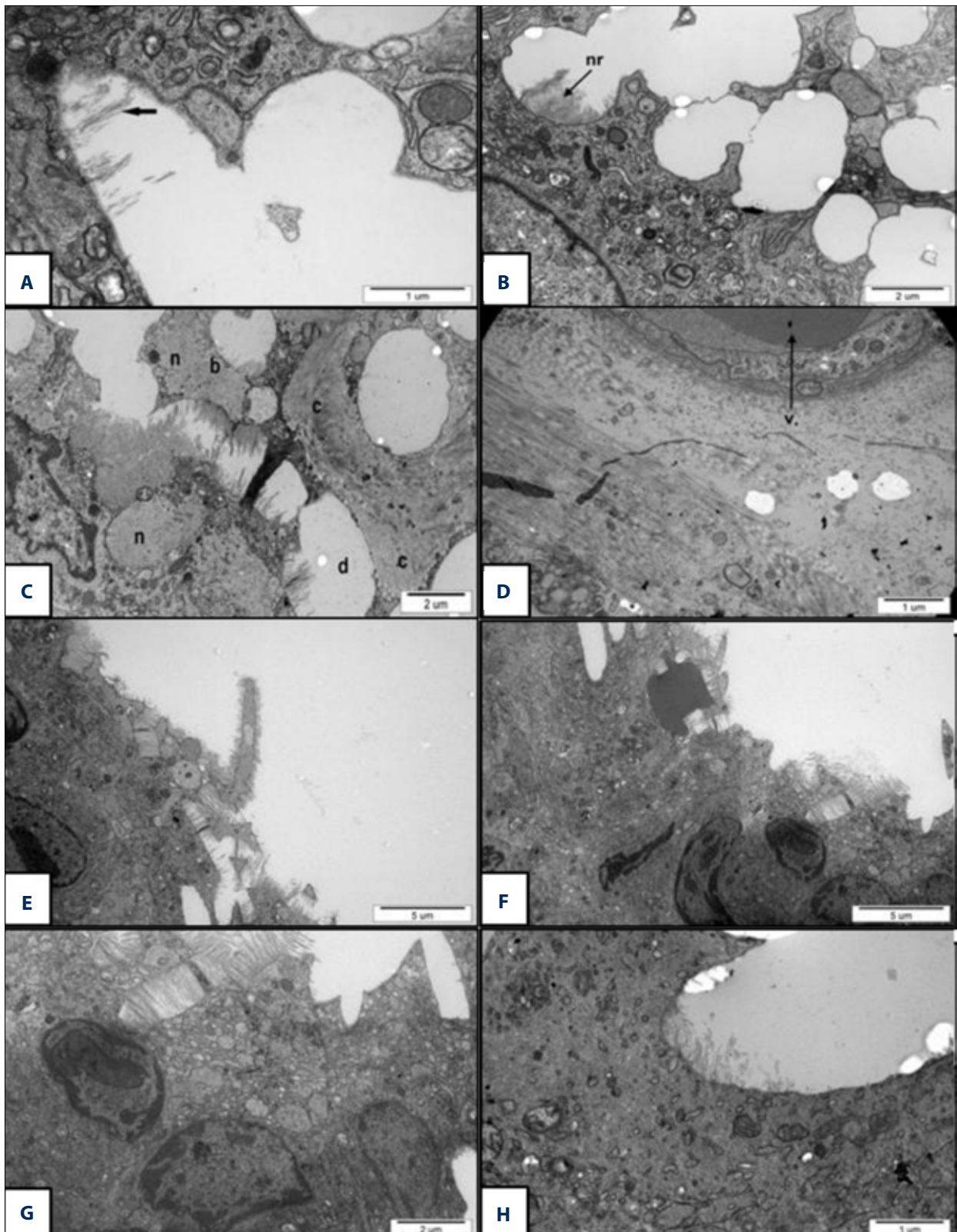


**Figure 5.** (A–H) Ultrastructural micrographs of specimen harvested from rat's peritoneum. The presented images show results obtained 6 weeks after implantation. Arrow points to bundles of collagen. nr indicates nanomaterial residue; b, border between collagen and nanomaterial; c, collagen; d, dissolved nanomaterial; n, niche filled with collagen; v, blood vessel lumen.

**Table 1.** Measured tensile properties of the PLCL tubular scaffold.

Material	Ultimate tensile strain (mm/mm)	Ultimate tensile strength (MPa)	Elastic modulus R1 (MPa)	Elastic modulus R2 (MPa)
PLCL	4.29	3.72	3.29	0.65

### TEM ultrastructural quantification of scaffold vascularization and degradation

Ultrastructural analysis of electrospun nanofibrous tubular scaffolds was performed following either subcutaneous or intraperitoneal implantation.

After subcutaneous implantation, a considerable amount of fibroblastic infiltration was noted (Figure 4C). The nearness of fibroblasts was expressed by multiple collagen fibrils. Adjacent graft cells demonstrated native morphology and structure. The focal oval structures presented in the ECM were remnants of nanofiber mesh (Figure 4A, 4B, 4D). The conduits were encased by collagen fibrils and native tissue, indicating degradation and remodeling/substitution of nanomaterial fibers by host tissues. On histological examination we observed the presence of young vascular capillaries (Figure 4E, 4F). Immunocompetent cells were not identified; however, fibroblast cells surrounded by collagen were present in the samples (Figure 4G). The large oval structures possessed a low number of nanofiber mesh remnants (Figure 4H). Fibroblast lamellipodia and collagen fibrils were directly connected with this oval structure. The large number of oval structures lacking identifiable nanomaterial suggests an intensified biodegradation process as opposed to replacement with connective tissue.

Specimens after peritoneal implantation analyzed by ultrastructure electron microscopy contained cells with appropriate morphology. Nanomaterial remnants were identified within the examined samples and can be seen in slides 5E, 5F, and 5G on Figure 5. A significant proportion of the samples demonstrated a large amount of degraded material (Figure 5H). The absence of macrophages and lymphocytes suggests the absence of an inflammatory response. The majority of the nanofibrous membrane had been dissolved during specimen fixation, but with varying levels of host tissue integration. The arrow on Figure 5A shows slight bundles of collagen fibrils replacing degraded electrospun membrane. On Figure 5B nanomaterial remnants can be observed. The border between proliferating elements of connective tissue and nanofibrous material is distinctly shown on Figure 5C, as indicated by the borders (b). Oval-shaped cavities of different sizes left by dissolved material are visible in the regions of less advanced integration of tissue with material (Figure 5C, 5D). This suggests a gradual integration of membrane into the host tissues. Collagen fibrils are seen filling uniformly oval-shaped niches. (Figure 5C;

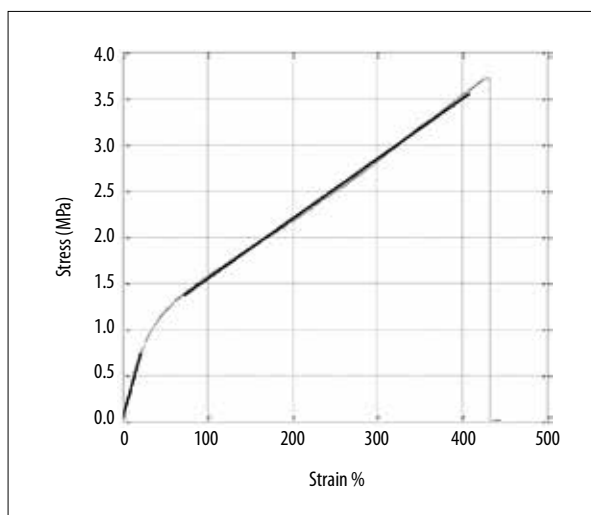


**Figure 6.** Stress/strain plot of the PLCL tubular scaffold. The stress/strain curves show two linear ranges in the material's behavior. The elastic range 1 was demonstrated up to 24% of strain, and the elastic range 2 between 70% and 429%.

n, niche). The niches, filled with ECM, are likely to be the traces of degraded nanomaterial. Absence of cells with abnormal structure or irregular pieces of membrane suggests good integration of the electrospun material with the surrounding tissue. Bridges of collagen fibrils are connecting regions of ECM. They are growing through nanomaterial, showing its gradual integration with surrounding host tissues. Fibroblasts surrounding the nanomaterial are producing collagen, which appears to be replacing the biodegraded nanomaterial. Proper blood vessels are formed in the nanomaterial (Figure 5D; v, blood vessel lumen). The specimens contain morphologically appropriate cells without evidence of an inflammatory response as well as nanomaterial in different stages of biodegradation (Figure 5A–5D); the above findings support adequate incorporation of the PLCL scaffold into the surrounding tissues.

### Mechanical properties of PLCL scaffold

The mechanical properties of the examined specimens can be found in Table 1. The stress/strain curves are depicted in Figure 6, showing two linear ranges in the material's behavior. The elastic range 1 was demonstrated up to 24% of strain and the elastic range 2 between 70% and 429%. The two regions were characterized by calculated elastic moduli.

The microscopic structure of the tested material demonstrated that the majority of fibers were positioned along the longitudinal axis of the specimen. Therefore, most of the fibers took part in transmission of the load imposed during the tensile test. However, in the fabrication process of the material, some of the fibers are mutually connected in a stochastic, pointwise manner, which may affect the elastic properties of the material. As shown in Figure 6, the material exhibited elastic behavior between 0% and 24% of strain, and furthermore a change in the properties was observed. The transition range can be interpreted as the process during which fibers reorganize and eventually tear the pointwise connections between them. The calculated values of the elastic moduli for both ranges are given in Table 1.

### Statistical analysis

The distribution normality of the parameter test in the peritoneum (Shapiro-Wilk normality test) and variance distinction (Snedecor F-test) justified the use of the Cochran-Cox parametric test. The average number of vessels following intraperitoneal implantation was found to be significantly higher compared to the average number in the subcutaneous implantation group as determined by the Cochran-Cox test ( $p < 0.0001$ ).

## Discussion

In the current study we examined an electrospun PLCL scaffold that is highly reproducible and develops interconnected pore networks, a graded mechanical stiffness, and tailored dimensions that can be designed to fit any tubular defect [13]. The PLCL construct prepared in this study has demonstrable biocompatibility and has been studied extensively in numerous animal models with respect to the body's response after subcutaneous, intraperitoneal, and urogenital applications [14]. Similar to previous studies, we found that pure scaffolds by themselves were able to induce angiogenesis [15]. Histological sections clearly demonstrated extensive angiogenesis compared with subcutaneous space. The membranes of electrospun nanofibers have been evaluated as a scaffolds for a wide variety of tissue-engineering applications including bone and urogenital [16–18]. Membranes of electrospun nanofibers have been tested as materials to prevent excessive scarring and to protect neural tissue following central nervous system surgery or injury, in addition to being used as a hemostatic dressing following kidney surgery. Nanofibers of conductive polymers are prospective materials for neural tissue engineering [19].

The polyesters used for nanofibrous scaffolds creation are approved for drug delivery systems (DDSs) and implants. Certain aliphatic polycarbonates are promising materials for tissue engineering and nanofibers due to their self-catalyzed degradation

resistance. Electrospun material used for tissue engineering does not induce a foreign body reaction after implantation due to its gradual degradation and replacement by the natural collagen matrix. Electrospun material could also have the potential to be recognized as native tissue if nanofibers were made of natural proteins.

Despite many successes in the field of bioengineering, the main limitation is the thickness of tissue structures. Only thin tissue structures like bladder or skin can be maintained by the diffusion of oxygen and nutrients from the host vasculature. When the thickness of scaffold exceeds 150–200  $\mu\text{m}$ , it will limit oxygen and nutrient diffusion, forming an unfavorable environment for cellular invasion and proliferation [13]. In the setting of limited oxygen diffusion, adequate incorporation of an implanted scaffold requires the development of a rapid, well-organized capillary network capable of providing the necessary nutrients in the interim [20]. After scaffold implantation, host blood vessels are prompted to invade the “tissue-forming” network in response to entrapped, hypoxic blood cells within the implanted construct [21]. Cell colonization and survival of biomaterials after implantation require a rapid, form-stable, functioning neovascular network that connects the implant to the recipient. In our study, we were able to characterize the angiogenic potential of the PLCL material using a wide array of techniques including biochemical/biophysical evaluation, TEM, and immunohistochemical analysis.

The largest obstacle to implant integration is the thickness of the biomaterial, which is directly related to the engineered materials' ability to become vascularized. Spontaneous vascular ingrowth is approximately several tenths of a micrometer per day [22]. With respect to the current state of knowledge, complete vascularization of several-millimeters-thick scaffold takes a couple of weeks. During this time, insufficient vascularization leads to hypoxia in the deeper tissue layers [23]. Furthermore, the variable nutrient and oxygen distribution within the scaffold results in a non-uniform cell differentiation and altered function of the newly created cells [15].

Bone marrow-derived endothelial progenitor cells have the potential to migrate into ischemic tissues in response to specific cytokines. Their localization in hypoxic regions triggers neovascularization [24]. The maturation process is combined with the suppression of endothelial cell activity. Proper timing is critical to establishing a physiologic vascular network/system.

Currently, numerous strategies for enhancing vascularization are under evaluation [25]. There are two main strategies aimed at increasing the rate of vascularization of an implanted biomaterial: the application of angiogenic growth factors (e.g., vascular endothelial growth factor [VEGF], fibroblast growth factor [FGF]) and creation of a structurally specific biocompatible

construct. The application of angiogenic growth factors such as FGF or VEGF or other on a biomaterial surface has been previously described [26]. However, there are limitations to their efficacy. Despite triggering endothelial cells and inducing angiogenesis, angiogenic factors have a paracrine effect and will have effects outside the area of interest [27]. Sustained angiogenic factor release may have untoward effects, with the putative ability to stimulate tumor growth or neovascularization in undesirable locations and/or at undesirable rates.

Another strategy is to create biomaterial with a structurally specific 3D construct that can be readily incorporated by the subject's own tissues [28]. Our previous research has clearly demonstrated that the arrangement of fibers facilitates the invasion of host endothelial cells, thus promoting angiogenic activity, especially in the intraperitoneal environment [29].

In nature, endothelial cell attachment is stimulated by the materials and structure that make up the ECM. Therefore, it is theoretically possible that an analogous, artificially created implant with a biomaterial makeup and structure similar to the ECM could induce the same programmed response of endothelial cell invasion, subsequent neovascularization, and eventual incorporation by the host tissues [30]. Furthermore, an added benefit of the current model is that PLCL has the ability to induce hydration and allow growth factors such as VEGF and FGFs to initiate specific biological processes including neo-angiogenesis and blood vessel maturation [31].

Electrospinning technology provides a unique opportunity to efficiently and reliably produce an artificial ECM substrate. Manufactured electrospun fibers can replicate the biochemical and structural ECM components necessary for incorporation [32]. Moreover, these PLCL fibers possess excellent mechanical properties with an appropriate time of biodegradation. Appropriate construction of PLCL material and its modification like increased hydrophobicity enabled strengthened cell adhesion to tested material [33].

## References:

- Kai D, Jin G, Prabhakaran MP et al: Electrospun synthetic and natural nanofibers for regenerative medicine and stem cells. *Biotechnol J*, 2013; 8: 59–72
- Feinberg AW: Engineered tissue grafts: Opportunities and challenges in regenerative medicine. *Wiley Interdiscip Rev Syst Biol Med*, 2012; 4: 207–20
- Smith IQ, Liu XH, Smith LA et al: Nanostructured polymer scaffolds for tissue engineering and regenerative medicine. *Wiley Interdiscip Rev Nanomed Nanobiotechnol*, 2009; 1: 226–36
- Kloskowski T, Jundzitt A, Kowalczyk T et al: Ureter regeneration – the proper scaffold has to be defined. *PLoS One*, 2014; 9: e106023
- Pokrywczynska M, Jundzitt A, Adamowicz J et al: Is the poly(L-lactide-co-caprolactone) nanofibrous membrane suitable for urinary bladder regeneration? *PLoS One*, 2014; 9: e105295
- Kloskowski T, Pokrywczynska M, Drewa T: Artificial urinary conduit construction using tissue engineering methods. *Cent European J Urol*, 2015; 68: 109–14
- Sill TJ, von Recum HA: Electrospinning: Applications in drug delivery and tissue engineering. *Biomaterials*, 2008; 29: 1989–2006
- Nakielski P, Kowalczyk T, Zembrzycki K et al: Experimental and numerical evaluation of drug release from nanofiber mats to brain tissue. *J Biomed Mater Res Part B Appl Biomater*, 2015; 103: 283–91
- Reneker DH, Yarin AL, Zussman E et al: Electrospinning of Nanofibers from Polymer Solutions and Melts. *Adv Appl Mech*, 2007; 41: 345–46
- Kowalczyk T, Nowicka A, Elbaum D et al: Electrospinning of bovine serum albumin optimization and the use for production of biosensors. *Biomacromolecules*, 2008; 9: 2087–90

Another novel technique currently being developed is to create an *in vitro* microvascular network within the biomaterial. An artificially created *in vitro* vascular network still requires host vascular integration. Predictions that a created *in vitro* network will connect with the host vascularization need be more thoroughly investigated. The more likely scenario is that endothelial cells are able to create a capillary network using a combination of angiogenic factors and biostructural surface-to-surface interactions [34]. Bioscaffold incorporation and neo-angiogenesis are a highly complex process controlled by a multitude of interactions between the ECM and different cell types, and interactions with the biomaterial itself [35]. Our observations stand in opposition to the currently held opinion that pure transplanted biomaterials manifest a low rate of incorporation and infiltration by the host vasculature [36]. This study showed that the use of biomaterials with angiogenic factors artificially incorporated prior to implantation and scaffolds seeded with endothelial cells prior to implantation is not crucial for angiogenesis and vascularization [37,38]. ECM conditions, material components, and 3D design of the scaffold fundamentally increase the rate of its vascularization [39,40].

Unfortunately, the latest results do not indicate clearly which strategy will be the best solution to fully revascularize tested biomaterial. In our opinion, future applications will likely require the incorporation of a multi-modal approach that includes a combination of all the aforementioned techniques.

## Conclusions

This study provides a unique, comprehensive approach to evaluating the prospective utilization of a PLCL scaffold in tissue regeneration. The scaffold design resulted in rapid vascularization propagation of the implanted biomaterial. The histological and mechanical data clearly demonstrate the putative potential of our PLCL construct in a variety of clinical applications including but not limited to the treatment of vascular and urological critical size defects.

11. Frontczak-Baniewicz M, Walski M: New vessel formation after surgical brain injury in the rat's cerebral cortex I. Formation of the blood vessels proximally to the surgical injury. *Acta Neurobiol Exp (Wars)*, 2003; 63: 65–75
12. Bodnar M, Szyłberg Ł, Kazmierczak W et al: Tumor progression driven by pathways activating matrix metalloproteinases and their inhibitors. *J Oral Pathol Med*, 2015; 44: 437–43
13. Cui X, Boland T: Human microvasculature fabrication using thermal inkjet printing technology. *Biomaterials*, 2009; 30: 6221–27
14. Woodruff MA, Hutmacher DW: The return of a forgotten polymer – Polycaprolactone in the 21<sup>st</sup> century. *Prog Polym Sci*, 2010; 35: 1217–56
15. Rouwkema J, Gibbs S, Lutolf MP et al: *In vitro* platforms for tissue engineering: Implications for basic research and clinical translation. *J Tissue Eng Regen Med*, 2011; 5: e164–67
16. Jin J, Park M, Rengarajan A et al: Functional motor recovery after peripheral nerve repair with an aligned nanofiber tubular conduit in a rat model. *Regen Med*, 2012; 7: 799–806
17. Kim S-H, Chung E, Kim S-H et al: A novel seamless elastic scaffold for vascular tissue engineering. *J Biomater Sci Polym Ed*, 2010; 21: 289–302
18. Shen J, Fu X, Ou L et al: Construction of ureteral grafts by seeding urothelial cells and bone marrow mesenchymal stem cells into polycaprolactone-lecithin electrospun fibers. *Int J Artif Organs*, 2010; 33: 161–70
19. Andrychowski J, Frontczak-Baniewicz M, Sulejczak D et al: Nanofiber nets in prevention of cicatrization in spinal procedures. Experimental study. *Folia Neuropathol*, 2013; 51: 147–57
20. Nguyen LH, Annabi N, Nikkiah M et al: Vascularized bone tissue engineering: Approaches for potential improvement. *Tissue Eng Part B Rev*, 2012; 18: 363–82
21. McCullen SD, Chow AGY, Stevens MM: *In vivo* tissue engineering of musculoskeletal tissues. *Curr Opin Biotechnol*, 2011; 22: 715–20
22. Moffa M, Polini A, Sciancalepore AG et al: Microvascular endothelial cell spreading and proliferation on nanofibrous scaffolds by polymer blends with enhanced wettability. *Soft Matter*, 2013; 9: 5529–39
23. Hutchings H, Ortega N, Plouët J: Extracellular matrix-bound vascular endothelial growth factor promotes endothelial cell adhesion, migration, and survival through integrin ligation. *FASEB J*, 2003; 17: 1520–22
24. Peichev M, Naiyer AJ, Pereira D et al: Expression of VEGFR-2 and AC133 by circulating human CD34(+) cells identifies a population of functional endothelial precursors. *Blood*, 2000; 95: 952–58
25. Chung S, Moghe AK, Montero GA et al: Nanofibrous scaffolds electrospun from elastomeric biodegradable poly(L-lactide-co-epsilon-caprolactone) copolymer. *Biomed Mater*, 2009; 4: 015019
26. Lee K, Silva EA, Mooney DJ: Growth factor delivery-based tissue engineering: General approaches and a review of recent developments. *J R Soc Interface*, 2011; 8: 153–70
27. Carmeliet P, Ferreira V, Breier G et al: Abnormal blood vessel development and lethality in embryos lacking a single VEGF allele. *Nature*, 1996; 380: 435–39
28. Gelain F: Novel opportunities and challenges offered by nanobiomaterials in tissue engineering. *Int J Nanomedicine*, 2008; 3: 415–24
29. Chen H, Fan X, Xia J et al: Electrospun chitosan-graft-poly (epsilon-caprolactone)/poly (epsilon-caprolactone) nanofibrous scaffolds for retinal tissue engineering. *Int J Nanomedicine*, 2011; 6: 453–61
30. Geckil H, Xu F, Zhang X et al: Engineering hydrogels as extracellular matrix mimics. *Nanomedicine (Lond)*, 2010; 5: 469–84
31. Zhou S, Gu L, He J et al: MDM2 regulates vascular endothelial growth factor mRNA stabilization in hypoxia. *Mol Cell Biol*, 2011; 31: 4928–37
32. Nair LS, Bhattacharyya S, Laurencin CT: Development of novel tissue engineering scaffolds via electrospinning. *Expert Opin Biol Ther*, 2004; 4: 659–68
33. Dhandayuthapani B, Yoshida Y, Maekawa T et al: Polymeric scaffolds in tissue engineering application: A review. *Int J Polym Sci*, 2011; 2011: 290602
34. Sunderkötter C, Steinbrink K, Goebeler M et al: Macrophages and angiogenesis. *J Leukoc Biol*, 1994; 55: 410–22
35. Jain RK: Molecular regulation of vessel maturation. *Nat Med*, 2003; 9: 685–93
36. Unger RE, Ghanaati S, Orth C et al: The rapid anastomosis between prevascularized networks on silk fibroin scaffolds generated *in vitro* with cocultures of human microvascular endothelial and osteoblast cells and the host vasculature. *Biomaterials*, 2010; 31: 6959–67
37. Ucuzian AA, Gassman AA, East AT et al: Molecular mediators of angiogenesis. *J Burn Care Res*, 2010; 31: 158–75
38. Yamamoto M, Rafii S, Rabbany SY: Scaffold biomaterials for nano-pathophysiology. *Adv Drug Deliv Rev*, 2014; 74: 104–14
39. Rouwkema J, Rivron NC, van Blitterswijk CA: Vascularization in tissue engineering. *Trends Biotechnol*, 2008; 26: 434–41
40. Moon JJ, West JL: Vascularization of engineered tissues: approaches to promote angiogenesis in biomaterials. *Curr Top Med Chem*, 2008; 8: 300–10